geosciences

MDPI

Article

Interpreting Soft-Sediment Deformation Structures: Insights into Earthquake History and Depositional Processes in the Dead Sea, Jordan

Bety S. Al-Saqarat [1,*], Mahmoud Abbas [2,*], Mu'ayyad Al Hseinat [1,3], Tala Amer Qutishat [1], Duha Shammar [4] and Ehab AlShamaileh [5]

[1] Department of Geology, School of Science, The University of Jordan, Amman 11942, Jordan; m.hseinat@ju.edu.jo (M.A.H.); talaqutishat@gmail.com (T.A.Q.)
[2] School of Geography and Tourism, Jiaying University, Meizhou 514015, China
[3] Department of Geophysics, Arab Center for Laboratory and Soil (ACES), Jeddah 23762, Saudi Arabia
[4] Environment, Water and Energy Research Center, Al al-Bayt University, Mafraq 25113, Jordan; duhashammar@aabu.edu.jo
[5] Department of Chemistry, School of Science, The University of Jordan, Amman 11942, Jordan; ehab@ju.edu.jo
* Correspondence: b.saqarat@ju.edu.jo (B.S.A.-S.); subariny_m2008@yahoo.com (M.A.)

Abstract: Soft-sediment deformation structures (SSDSs) typically form in unconsolidated sedimentary deposits before lithification. Understanding these structures involves evaluating their characteristics, genesis timing, and the dynamics of sediment deformation. SSDSs are essential for deciphering ancient environments, reconstructing depositional processes, and discerning past prevailing conditions. In the Dead Sea region, SSDSs are abundant and well preserved due to unique geological and environmental factors, including rapid sedimentation rates and seismic activity. Influenced by the Dead Sea Transform Fault, the area offers insights into tectonic activity and historical earthquakes predating modern instrumentation. This study extensively examines SSDSs along the Dead Sea area in Jordan, focusing on sediments near the Lisan Peninsula, where the prominent Lisan Formation (71–12 ka) exposes numerous deformations. Mineralogical and geochemical analyses using X-ray diffraction (XRD) and X-ray fluorescence (XRF) were applied on deformed and undeformed layers to test the potential trigger of seismite formation in the Dead Sea area. The XRD and XRF results reveal Aragonite and Halite as the predominant compounds. Field observations, coupled with mineralogical and geochemical data, suggest tectonic activity as the primary driver of SSDSs formation in the Dead Sea region. Other contributing factors, such as high salinity, arid climate, and depositional settings, may also have influenced their formation. These structures offer valuable insights into the region's geological history, environmental conditions, and tectonic evolution.

Keywords: soft-sediment deformation; Dead Sea Transform Fault; Jordan; earthquakes; depositional processes

Citation: Al-Saqarat, B.S.; Abbas, M.; Al Hseinat, M.; Qutishat, T.A.; Shammar, D.; AlShamaileh, E. Interpreting Soft-Sediment Deformation Structures: Insights into Earthquake History and Depositional Processes in the Dead Sea, Jordan. *Geosciences* **2024**, *14*, 217. https://doi.org/10.3390/geosciences14080217

Academic Editor: Rosa Nappi

Received: 22 May 2024
Revised: 31 July 2024
Accepted: 9 August 2024
Published: 16 August 2024

1. Introduction

Soft-sediment deformation structures (SSDSs) manifest within unconsolidated sedimentary deposits before lithification occurs, offering valuable insights into depositional conditions and pre-consolidation processes [1–6]. These structures, which have formed relatively recently, are found across a variety of environments, including glacial, deep marine, lacustrine, fluvial, aeolian, and evaporitic settings [1,7–11].

Various processes, such as fluidization and liquefaction, contribute to the formation of SSDSs when water between the grains exceeds the confined pressure above the top of the layer, causing liquefaction [12–15]. Factors triggering liquefaction include earthquakes, shear stress along sediment–water interfaces, groundwater table fluctuations, sediment overloading, and rapid sedimentation [16–20]. These deformational processes, often devoid

of structural or morphological evidence post-liquefaction, provide valuable insights into preserved seismic events within sedimentary records [1,5,7,11,17,21–25].

The Dead Sea Basin (DSB) stands as a significant sedimentary archive in the Mediterranean region, with sedimentary characteristics reflecting climatic and environmental variations, particularly during the Quaternary period [26,27]. Moreover, the Dead Sea Transform Fault (DSTF) significantly influences sedimentary structure development through deformation and subsidence [28,29]. SSDSs are widespread in the Dead Sea area, notably within the Lisan Formation deposited in the lacustrine environment, composed primarily of alternating carbonate and detrital laminae, laminated detritus, and laminated halite facies [30]. However, understanding of the factors contributing to the formation and evolution of such sedimentary deformations, whether through seismic activities or other diagenetic processes, remains limited.

This study aims to investigate SSDSs across the Dead Sea region of Jordan (Figure 1A,B), with the goal of elucidating the processes underlying their formation. Our understanding of the formation and evolution of the SSDSs in the region, along with their deformational style, contributes to the knowledge of their lithological, sedimentological, mineralogical, and geochemical characteristics.

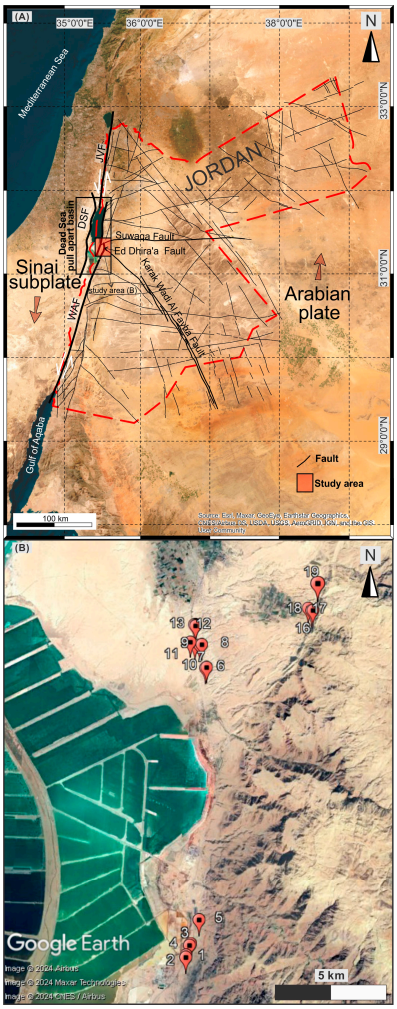

Figure 1. (**A**) Location map of Jordan (dashed red line) exhibits the major structural elements, including the DSTF segments (based on [31,32]). The plate tectonic configuration of the region is modified from Stern and Johnson [33]. DSF: Dead Sea Fault; JVF: Jordan Valley Fault; WAF: Wadi Araba Fault [31–33]. (**B**) Satellite image showing the locations of the nineteen studied outcrops of SSDSs in the Dead Sea area.

2. Geological and Tectonic Setting of The Study Area

The DSTF system is one of the world's longest active sinistral strike-slip fault systems that extends ~1100 km (Figure 1A) [28,34], marking the boundary between the Arabian plate and the Sinai subplate [35–37]. It is characterized by a series of deep, narrow, and elongated basins, including the Dead Sea pull-apart basin. The DSTF dates to ~14 Ma (middle Miocene) and has accommodated ~105 km of left-lateral displacement [28,38,39]. Kinematically, the plate movement along the DSTF involves both strike-slip and dip-slip components, which played a crucial role in the formation and evolution of the Dead Sea (Figure 1A) [28]. The convergence of the African-Sinai plate and Arabian plate has resulted in the formation of a deep rift valley (790 m b.s.l maximum depth), known as the Dead Sea Rift. The vertical rifting produced a series of step faults that form the lateral hills staggering along both sides of the Dead Sea Rift. The vertical movement of the rifted areas to the bottom of the valley is about 10 km, while the relative uplift of the surrounding margins of the fault (filled rift) is about 1.5 km (e.g., [28,38,39]).

It is well documented that the orientation of stress fields in the northwestern Arabian plate underwent multiple shifts from the Turonian period to the present day. For instance, it transitioned from a WNW-ESE compression linked with the Syrian Arc Fold-Belt system (Turonian–Plio-Pleistocene) [40] to an NNE-SSW extension associated with the opening of the Red Sea (Neogene–present day) [41]. The structural configuration of the northwestern Arabian plate was significantly shaped by a substantial N-S extensional stress regime attributed to the Irbid rift, which began during the Oligocene–Early Miocene period (~25–17 Ma) and persists to the present day [41,42]. This extension is attributed to various factors, including the Afar mantle plume, the Red Sea opening, sub-lithospheric northward flow, and extensive volcanism across the Arabian plate (Harrat Ash Shaam Basalt) [42–49]. Concurrently, NW-trending rifting occurred along the Wadi Sirhan Graben during the Cretaceous period, which was reactivated during the Oligocene period and has persisted since then [49].

Situated within the Dead Sea Rift, the DSB occupies a pivotal position and exhibits a remarkably rapid rate of subsidence, resulting in the continuous deepening of its basin floor [50]. The basin's asymmetry is evident, with steep cliffs dominating its western flank and a more gradual slope characterizing its eastern counterpart [28].

Over geological time, the basin and the neighboring areas [51,52] have become occupied by several lakes, with the most recent predecessors being Samra Lake during the last interglacial period (71–29 ka) and Lisan Lake during the last glaciation (12–71 ka), ultimately evolving into the present-day Dead Sea Lake [50,53]. These lakes, alongside earlier occupants of the DSB, have left behind unique sedimentary records in the region (Figure 2). Furthermore, the Dead Sea's sensitivity to Mediterranean climate fluctuations [54] led to variations in the hydroclimate record across the basin [26]. The Lisan Lake level has fluctuated through the late Pleistocene due to changes in the hydroclimate of the Mediterranean region [27]. The recession of the Lisan Lake triggered a series of geological events that shaped the current landscape of the region. As the lake level receded, it left behind extensive deposits of gypsum and aragonite, forming distinct terraces along the shores of the Dead Sea and on the Lisan Peninsula [55,56]. This study focuses on examining these preserved geological structures, particularly the gypsum and aragonite terraces, to assess their relevance to the seismic history of the Dead Sea area. By analyzing the characteristics, composition, and distribution of these terraces, we aim to gain insights into the occurrence and magnitude of past seismic events that have impacted the region.

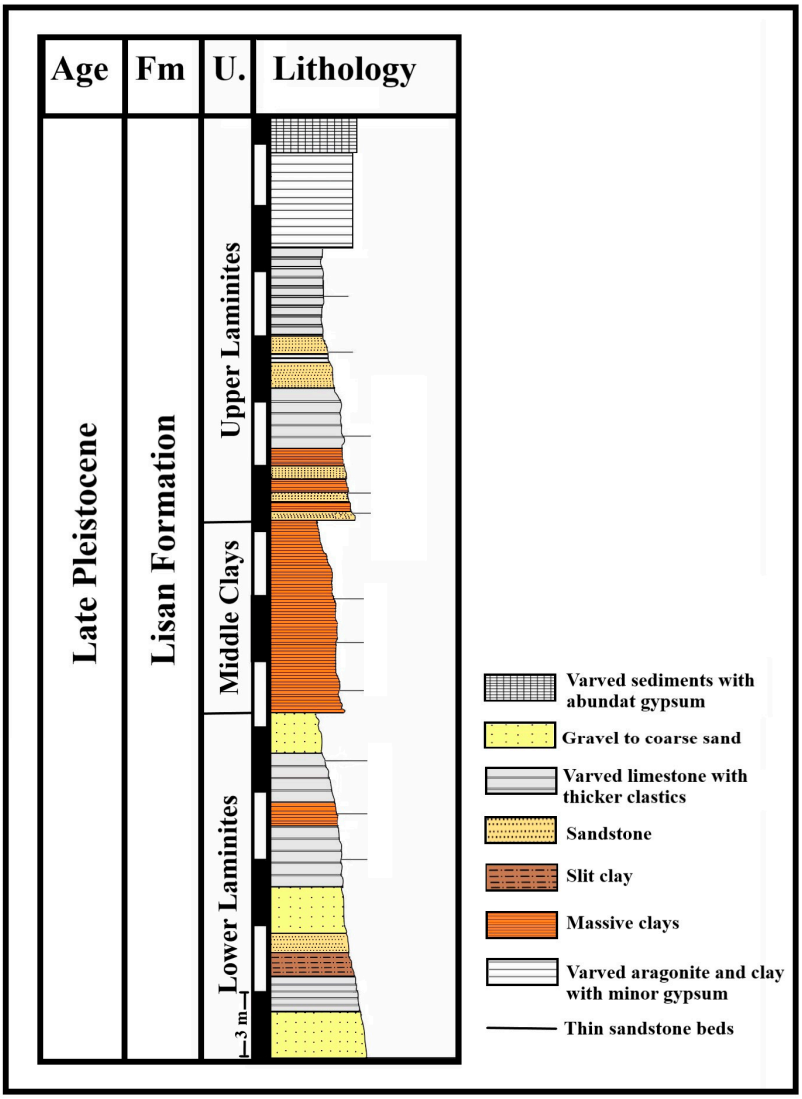

Figure 2. Stratigraphic column of the Lisan Formation in central Jordan (modified after Abed and Yagan [57].

The geological diversity of the Dead Sea area is further showcased by its varied landscape, encompassing salt flats, sinkholes, and mineral-rich muds. Ongoing tectonic movements along the DSTF persistently mold the region's geology, contributing to its dynamic character. Overall, the tectonic and geological configurations of the Dead Sea epitomize a captivating illustration of Earth's geological processes in action.

3. Materials and Methods

3.1. Sedimentary Sections

SSDSs are well preserved within the Lisan Formation along the Dead Sea region, exhibiting varying sedimentary characteristics from the northern to the southern stretches of the Dead Sea. For this study, representative nineteen sites were selected on the eastern side of the southern basin of the Dead Sea near the Lisan Peninsula (Figure 1B). The Lisan Formation in this area, comprises Lisan Marl and Lisan Marl Gravel, approximately 25–30 m depth, and is composed of laminated beds featuring aragonite, gypsum, clay, and detrital sediments. Certain outcrops display repetitive cycles of gravel, sediments, and laminated fine to medium-grained pink sandstone interspersed with pebbles. Major faults such as the DSTF, Karak Wadi Al Fayha Fault, and Ed Dhira'a Fault are influencing the geology and the landscape of the Dead Sea Basin.

The SSDSs in the Dead Sea vicinity exhibit alternating layers of limestone and detrital sediment, as well as laminated detritus and salt facies. These sedimentary patterns stem from the fluctuating lake levels during the late Quaternary period, corresponding to glacial and interglacial cycles [58]. Specifically, limestone and detrital layers formed during glacial phases when the lake was at higher levels [59], while salt facies emerged during interglacial periods when the lake reached its lowest points [60].

Within the study area, the Lisan Formation is characterized by laminated beds primarily consisting of sediments of chemical origin deposited from Lisan Lake. The thickness of individual laminated layers ranges from a few millimeters, with black and white laminae comprising limestone and gypsum, respectively, reflecting seasonal variations [61].

3.2. Experimental Methods

Major and trace element compositions in laminated sedimentary within the Dead Sea region were analyzed by X-ray fluorescence spectrometry (XRF) using a Shimadzu XRF-1800 spectrometer. Two samples were collected from both deformed (DST1, Figure 3C) and undeformed (DST2, Figure 3D) sedimentary layers to assess the presence or absence of specific elements associated with deformation processes and to investigate the geochemical characteristics of these laminated layers. The XRF analysis enabled the identification of a range of oxides, including CaO, SiO_2, Al2O_3, Fe_2O_3, MgO, Cl, SrO, K_2O, SO_3, Na_2O, TiO_2, P_2O_5, MnO, Cr_2O_3, and CuO. The XRF samples underwent additional verification through XRD analysis to confirm their mineralogical composition and explore diagenetic formation, providing insights into mineralogical alterations occurring during deformational processes. X-ray diffraction (XRD) patterns of samples were obtained using a Shimadzu MAXima-X XRD-7000 automatic diffractometer. Thin sections were investigated by a polarizing microscope Nikon Eclipse LV 100 Pol (2 theta ranges between 3 and 63 deg) to identify the composition of both deformed and undeformed layers. The analyses were carried out at the Hashemite University, Jordan.

4. Results and Interpretations

4.1. SSDSs in the DSB

Various types of soft-sediment deformations within the laminated layers along the Dead Sea area were examined during field investigations. In the sections below, we provide a description for each type.

4.1.1. Small-Scale Slumps

This type of deformation in the Dead Sea area is characterized by folded and unfolded laminated layers (Figure 3A–E). Numerous exposures were observed, primarily within the laminated beds of the Lisan Formation composed of aragonite-bearing carbonates and dark clay layers. Several outcrops were examined near the potash ponds on both sides of the highway and in some narrow valleys. The size of the slumps ranged between millimeters and a few centimeters, except for those reported in Figure 4A, which reached the size of 10 cm. This is due to the aftershock seismic activity being applied prior to lithification in a short period, indicating that the epicenter of the earthquake was close [62]. The thickness of the deformed layers sandwiched between two undeformed layers varied from one location to another, indicating the degree to which these layers were not fully consolidated during deposition and were subsequently exposed to seismic activity prior to solidification.

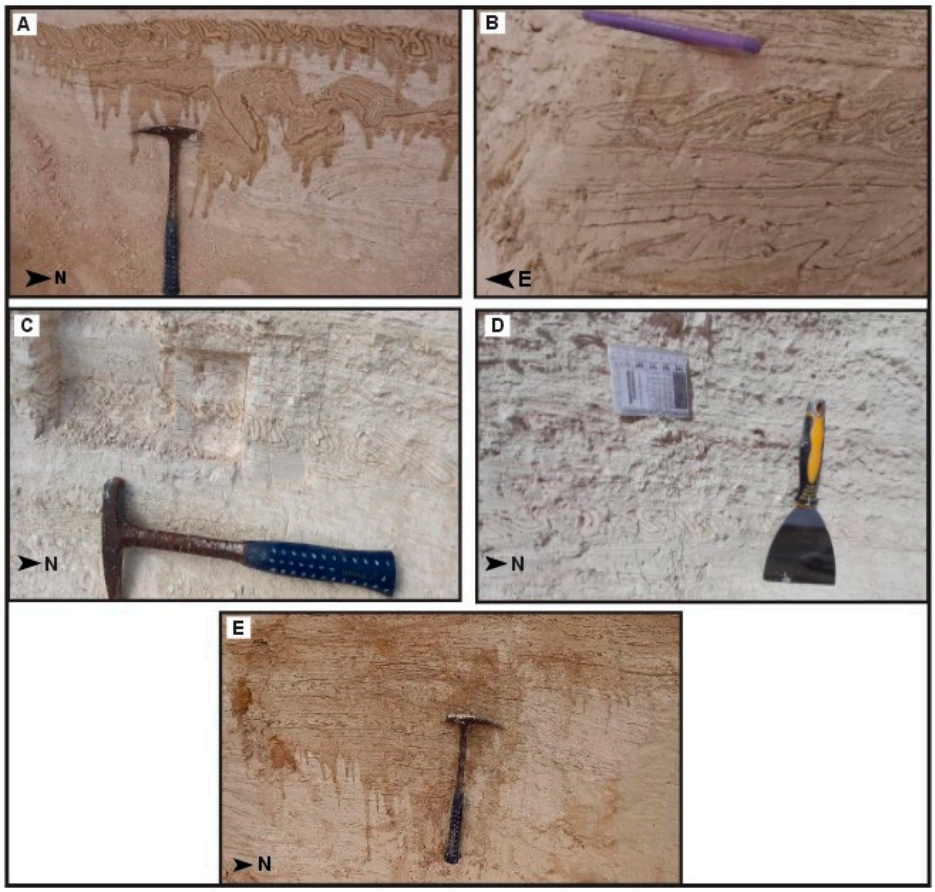

Figure 3. (**A**) Two deformed beds with southward verging slumps of variable size (31°14′6.1″ N, 35°31′12.20″ E; site 15). (**B**) One of the deformed layers with westward verging slumps (31°14′6.10″ N, 35°31′12.20″ E; site 11). (**C**) Deformed layer between two undeformed layers (31°13′38.70″ N, 35°31′6.80″ E; site 15). (**D**) Two deformed layers separated by undeformed layer (31°14′5.03″ N, 35°31′14.97″ E; site 13). (**E**) Four deformed beds with slumps and with different thicknesses and wavelengths (31°14′5.03″ N, 35°31′14.97″ E; site 13). The length of the hammer is 41 cm, the pen is 11 cm, and the shovel is 22 cm.

The presence of laminated limestone and mud within the Lisan Formation, exhibiting folds with varying degrees of deformation, suggests distinct stages of deformation. These layers are typically deposited under conditions of low sedimentation energy, with increasing density towards the bottom to mitigate the effects of gravitational instability, such as Rayleigh–Taylor instabilities [63]. Notably, the laminated layers display a parallel displacement process, which is uncommon in soft sediments and typically requires shear forces associated with various mechanisms, like Kelvin–Helmholtz instabilities [64]. Such lateral shear forces may result from fluid passage after sedimentation or the presence of a slope on which sediments were deposited.

4.1.2. Mixed Layer

This structural feature was observed in two outcrops within the study area (Figure 4A,B), characterized by the presence of two distinct components within a single layer consisting of sand and laminated marl beds. The thickness of the mixed layer was approximately 60 cm and 40 cm, with the degree of mixing diminishing. The interaction between the sand and marl layers occurred due to density variations, with the sand layer influencing the laminated marl layer. Within the mixed marl layer, fragments were observed brecciated into various-sized pieces, while the sand layer exhibited a mushroom (diapiric) shape. Furthermore, the layers above the semi-horizontal mixed layer of gravel, marl, and sand

displayed a decrease in the number of fragments towards the top, while the layer beneath the mixed layer slid downwards, evident by the accumulation of broken marl pieces.

The formation of a mixed layer occurs when horizontal laminae are liquified, broken into fragments, suspended, and then re-deposited [65]. Various factors may contribute to the formation of such mixed layers, including earthquakes, river flows, and layer slippage [66]. River flow, as a potential cause, was dismissed since the fractured sediments originated from the laminated marl and not from a river source, and the layer above the mixed layer, consisting of gravel, remained unaffected by deformation. Moreover, tracing the layer laterally revealed that horizontal layers remained unaffected by deformation, indicating that river flow was not responsible for the deformation of the mixed layer. Additionally, the pieces of marl were re-deposited in the same location without undergoing any transformation processes. Therefore, it is probable that the formation of this mixed layer resulted from a seismic event coinciding with density inequality between the sand and marl layers.

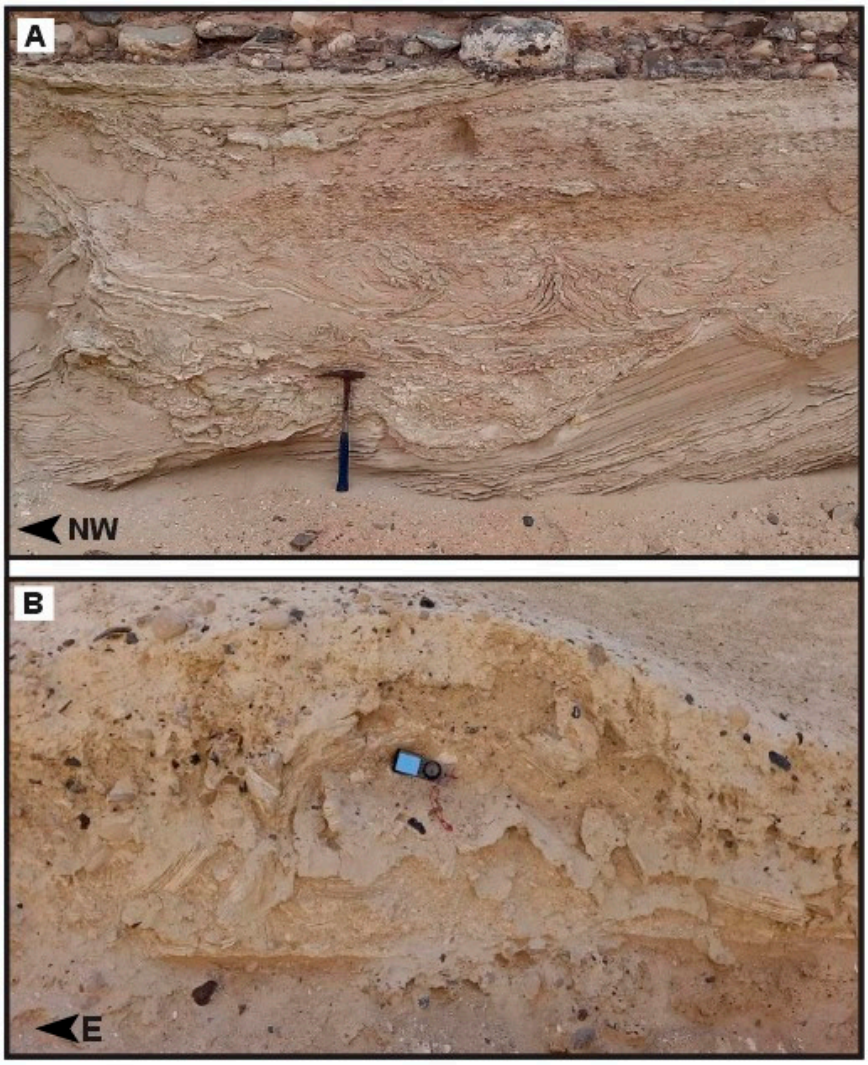

Figure 4. (**A**) Mixed layer contains diapir fragments of marl mixed with sandy layer (31°6′1.60″ N, 35°31′36.10″ E; site 4). (**B**) Mixed layer showing fragments of course- and fine-grained sediments (31°6′1.60″ N, 35°31′36.10″ E; site 4). The length of the hammer is 41 cm and of the Silva compass is 17 cm.

4.1.3. Cross-Cutting Injection Dikes and Neptunian Dykes

Injection dikes, a term used to describe structures formed by fluidization resulting from over-pressurized sediments along hydraulic fissures, are known to occur during earthquakes [66–70]. These injection dikes were observed in two outcrops (Figure 5A,B). As the thickness decreases downward, evidence of multiple flows is indicated, leading to the classification of this structure as a "Neptunian dyke" [71]. Additionally, at another outcrop, the injection dyke material consisted of clay and penetrated hard layers of laminated marl.

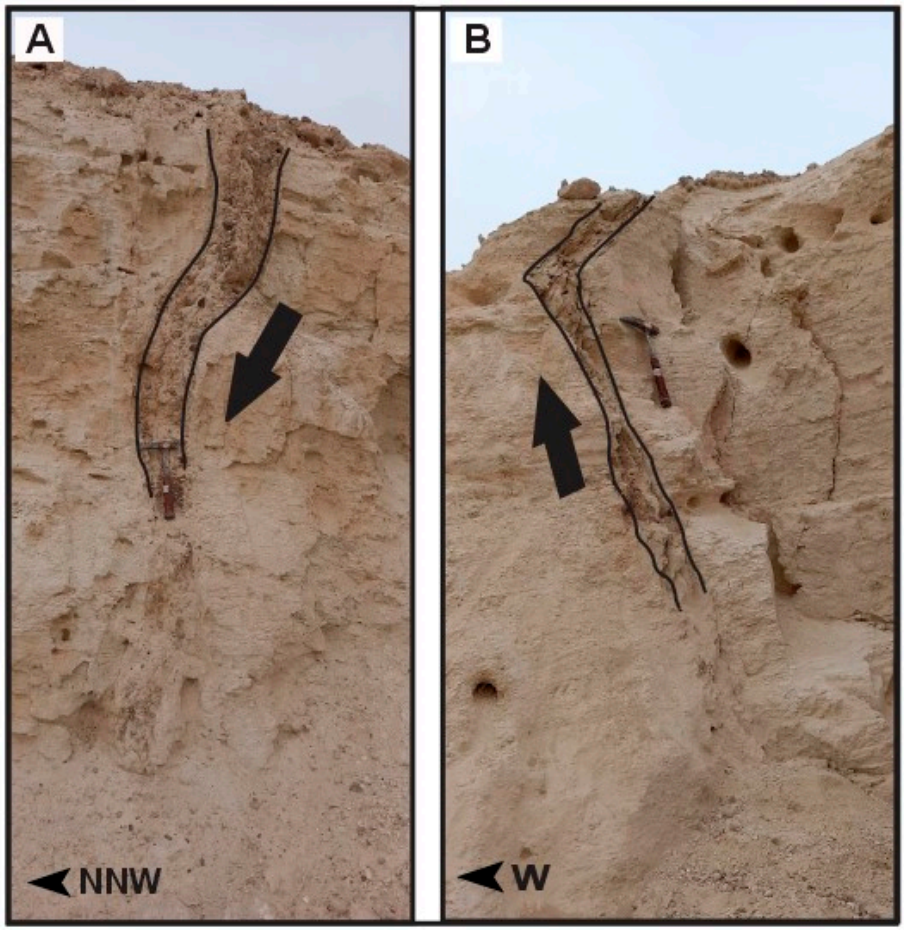

Figure 5. (**A**) Neptunian dyke: the arrow indicates the direction of sediments flow from the top to the bottom as evidenced by decreased width of the dyke with depth (31°13′34.60″ N, 35°31′15.40″ E; site 10). (**B**) Injection dyke: the arrow indicates the direction of the flow of liquified sediments from bottom to the top of the stratigraphic section (31°14′6.10″ N, 35°31′12.20″ E; site 15). The length of the hammer is 33 cm.

These dikes form due to fluid or water infiltration, resulting from vertical sediment movement that has undergone fluidization or liquefaction. Water and fluids infiltrate between the layers through cracks formed by shear stress induced by the pressure from the pores during the fluidization and liquefaction process [14,67]. The driving force behind the formation of these injection dikes is the result of gravitational instability and shear processes, causing fluidized and liquefied sediments to flow upward [72]. In Neptunian dykes, these structures are generated by the expansion of solidified and cohesive sediments, with subsequent cracks being filled with sediments [71].

4.1.4. Load and Flame Structures

Numerous instances of these structures were observed in two outcrops (Figure 6A,B), where they appeared to form through the deposition of layers with higher density than the disturbed layer. Layers consisting of fine to medium-grained sand mixed with pebbles were noted atop marl layers of lower density. This resulted in the intrusion of fine to medium-grained sand into the overlying marl bed under unstable conditions, giving rise to flame-like shapes that seem to have formed post-deposition. The flame structure, resembling a snake head or tongue shape, spans several centimeters in height and width. This intrusion occurs due to reverse density gradation, with plastic intrusion of underlying liquefied and fluidized sediments occurring into the overlying coarser sand and clay bed. The source bed of sand and mud lies at the bottom sequence, and the structure extends into the overlying clay unit due to the expulsion of pore water by liquefaction and loading of the lower layer. Load structures were also observed in another two outcrops, where a layer of gravel affected a layer of marl, leading to the formation of these structures.

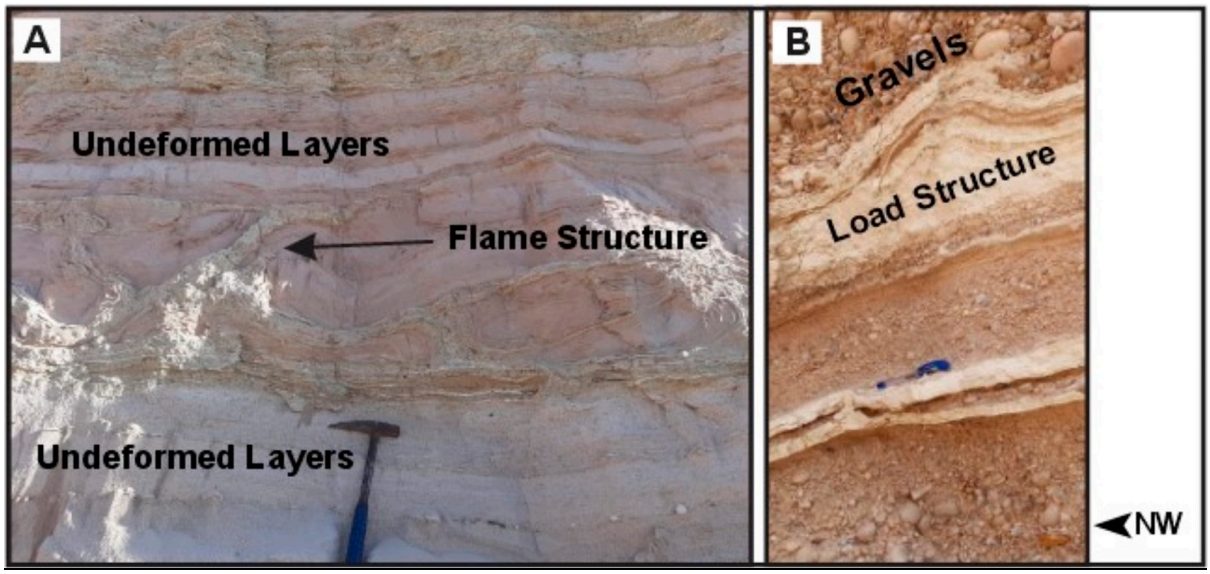

Figure 6. (**A**) Load and flame structures (31°6′4.10″ N, 35°31′37.80″ E; site 3). (**B**) Load structure (31°6′4.10″ N, 35°31′37.80″ E; site 3). The length of the hammer is 41 cm and of the pen is 14 cm.

Load structures formed because of density inversion at the boundary between a liquefied sedimentary layer and a layer with high bulk density [71–73]. The final form of these structures depends on various factors, including the actual density of the layer with high density, the viscosity of the deformed layer affected by deformation, and the duration of the liquefaction process [68]. Formation of these structures is facilitated by regional earthquakes or tangential stress resulting from sudden sediment emplacement [13,14,72].

4.1.5. Fragile Clast

Figure 7 shows a fragile clast, where a layer of laminated marl was incorporated with the overlying cap layer, consisting of fine to medium-grained sandstone. Their formation occurs prior to the sedimentary layer's consolidation atop the distorted layer. It may also result from local folding of these structures, subsequent re-deformation, and eventual merging with the upper sedimentary cover due to deformation processes in soft sediments associated with individual mass transport deposition [74].

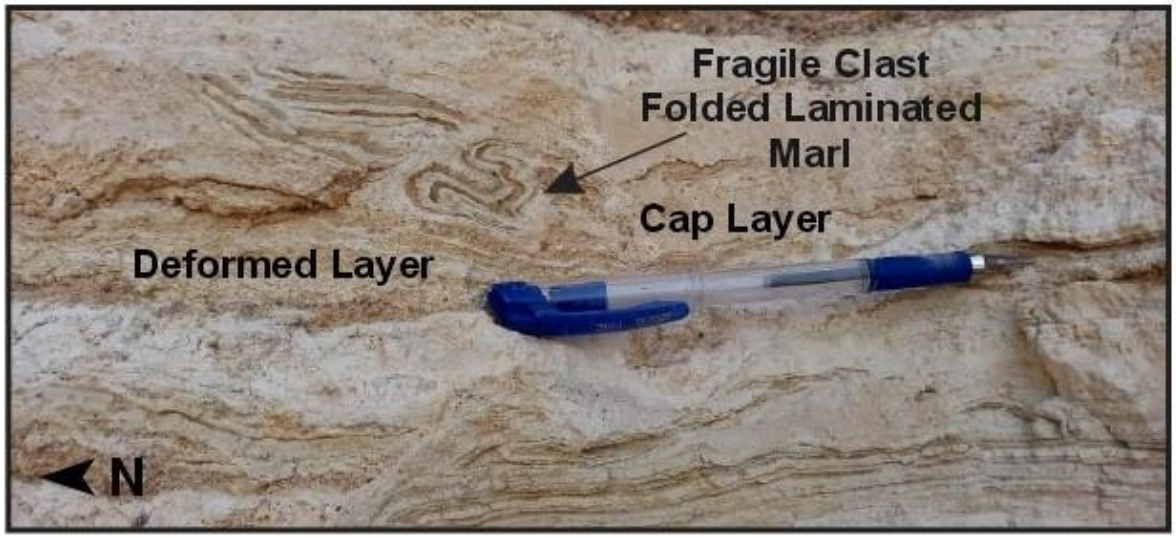

Figure 7. Folded laminated marl that incorporates a cap layer of fine to medium-grained sandstone (31°13′34.60″ N, 35°31′15.40″ E; site 10). The length of the pen is 14 cm.

4.2. Mineralogical Analysis

The XRD analysis results indicated that the undeformed layer primarily contained the following major minerals: Aragonite-$CaCO_3$, Halite-NaCl, and Graphite-C (Figures 8A and 9A). Conversely, the layer affected by syn-sedimentary deformation comprised Aragonite-$CaCO_3$, Calcite-$CaCO_3$, and Graphite-C (Figures 8B and 9B). The thin laminations exhibited a highly crystalline Calcite-Aragonite composition.

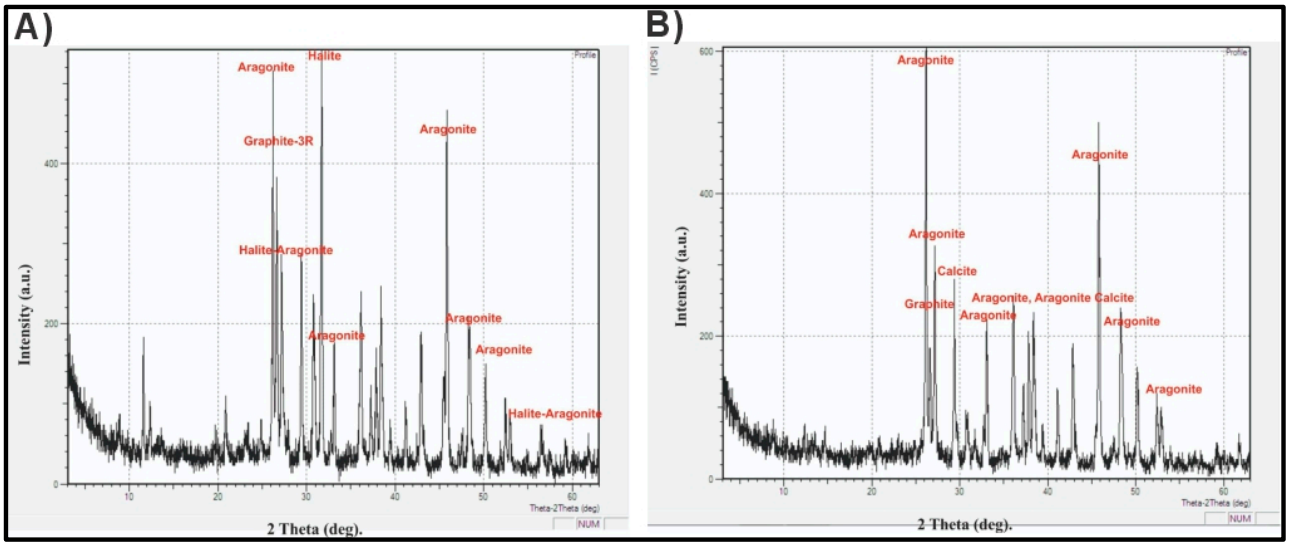

Figure 8. (**A**) XRD results for the major minerals in the undeformed layer (DST1). (**B**) XRD results for the major minerals in the deformed layer (DST2).

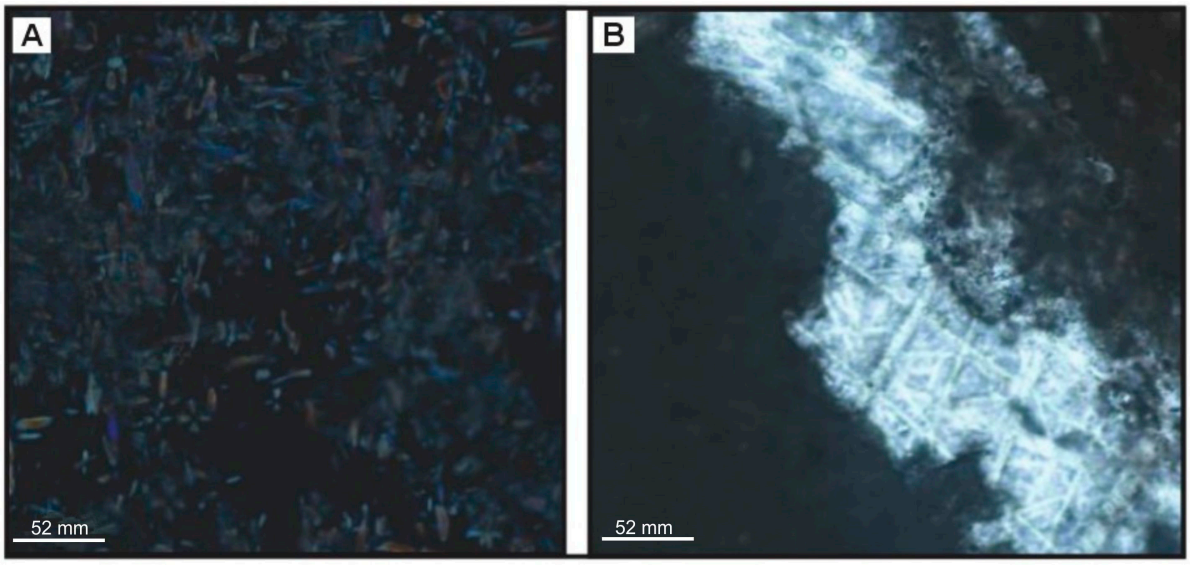

Figure 9. (**A**) Thin section reveals 10× zoom to aragonite crystals in undeformed layer. (**B**) Thin section 10× zoom of aragonite crystals in deformed layer.

4.3. Geochemical Analysis

XRF analysis of the samples reveals that both the deformed and undeformed layers contained identical chemical compounds, including CaO, SiO_2, Al2O_3, Fe_2O_3, MgO, Cl, SrO, K_2O, SO_3, Na_2O, TiO_2, P_2O_5, MnO, Cr_2O_3, and CuO, with similar proportions (Table 1). The high percentage of CaO detected in the XRF analysis suggests a predominance of aragonite minerals, as indicated by the XRD analysis. Additionally, the presence of the remaining elements indicates the presence of detrital sediments within the laminated aragonite/detrital facies.

Table 1. XRF analysis results for deformed and undeformed layers.

Compound	Chemical Formula	Percentage (%) (Undeformed)	Percentage (%) (Deformed)
Calcium oxide	CaO	46.37%	44.27%
Quartz	SiO_2	6.82%	8.93%
Aluminum oxide	Al_2O_3	2.19%	2.85%
Iron oxide	Fe_2O_3	1.49%	1.92%
Magnesium oxide	MgO	1.43%	1.64%
Chlorine	Cl	1.34%	1.51%
Strontium oxide	SrO	1.32%	1.21%
Potassium oxide	K_2O	0.72%	0.94%
Sulfur trioxide	SO_3	0.71%	0.77%
Sodium oxide	Na_2O	0.63%	0.65%
Titanium dioxide	TiO_2	0.2%	0.30%
Phosphorus pentoxide	P_2O_5	0.10%	0.10%
Manganese oxide	MnO	0.02%	0.03%
Chromium oxide	Cr_2O_3	0.02%	0.02%
Copper oxide	CuO	0.01%	0.00%

5. Discussion

5.1. Sedimentological and Lithological Settings of the SSDSs

Laminated layers in the Dead Sea area are referred to as "varve" deposits that are formed due to seasonal annual sedimentation and its formation mainly relied on the freshwater input to the basin [30,75,76] However, the age of these sediments could be achieved using radiometric dating methods such as U/Th and radiocarbon dating methods applied on carbonate sediments [76,77]. Therefore, the laminated layers in the Dead Sea area could play a pivotal role in reconstructing the Dead Sea Lake level history [30,53,58,59]. Yet, the evaluation of the laminated layers in the Dead Sea area called "varves" is still a debated topic [30,76,77]. Further microfacies investigations should be carried out to understand its formation.

SSDSs are saturated and unconsolidated sediments that form immediately after their deposition over a short period [5,78,79]. Originally, the deformations were caused by their loss of shear strength, which could lead to liquefaction, fluidization, and thixotropy [5,22,80]. Deformations in soft sediments also occur in volatile water environments, especially those in which groundwater is found. In addition, these deformations are caused by rapid sediment load, tidal shear, freeze–thaw conditions, and gravity flows [4,16,22,81,82].

The presence of seismites in modern sediments is considered as evidence of tectonic activity of the Dead Sea Rift [11]. The sediments of the Dead Sea are characterized by striking sedimentary deformations and frequent earthquakes. These distortions passed several stages. Initially, layers deposited horizontally, signifying a static stage before the earthquake. Subsequently, they turned into medium folded layers, followed by oblique folding, asymmetric folding layers, coherent vortices, and turbulent chaotic structures [83].

In the Dead Sea area, SSDSs have been formed by a combination of processes, such as groundwater movement and, most importantly, seismic activities. The fieldwork observations carried out in the study area indicate that these processes were the major components of the formation of the SSDSs. The liquefaction process is mainly triggered by groundwater movement which is considered as the main forcing mechanism causing SSDSs. The groundwater depth of the Dead Sea/Wadi Araba Basin ranges between a few meters to tens of meters. Hence, it does not appear that the shear stress force triggered by the groundwater movement influences the formation of the SSDSs in this area.

5.2. Seismically Induced Soft Sediment Deformations (SSDSs)

The formation of the SSDSs in the Dead Sea area might be attributed to seismic activities. The formation of SSDSs requires seismic waves that occur due to an earthquake with a magnitude of $\geq$5.5 ML [84]. Nevertheless, it is reported that the average earthquake recurrence period is about 340 $\pm$ 20 yr with magnitudes of $\geq$5.5 ML, according to a study of the seismic disturbances that affected Lisan's sediments, specifically on the eastern side of the Dead Sea in Wadi Arab [7]. Several structural features including truncated folds and cross-cutting clastic dykes were recognized in the Lisan Formation sediments, which are indicative of the deformation [85,86]. With regard to small-scale slump folds moving it vertically and continuing laterally, it has obtained what are called "seismites", that is, they were caused by the earthquake. Additionally, many measurements of strike and dip were taken of small faults scattered in the study area, where it was observed that they correspond to the general trend of the DSTF and the Karak Wadi Al Fayha Fault, as these faults have affected these Quaternary sediments [87,88]. Few local geologists in Jordan delved into the study of seismically induced SSDSs, as seen in the works of El-Issa and Mustafa [7] and Amaireh [11]. El-Issa and Mustafa [7] scrutinized SSDSs within the Lisan Formation, attributing the deformations to the movement of the Wadi Araba Fault. Conversely, Amaireh [11] examined similar deformations in the northeastern corner of the northern DSB, associating them with local fault activity in the region. Contrastingly, extensive research on SSDSs and their correlation with the DSTF movement has been conducted on the western shore of the Dead Sea.

The presence of folded, deformed, eroded, and truncated layers indicated the occurrence of syn-sedimentary deformations. These deformations occur at the interface between the sediment and water, immediately after the deposition of the deformed layer and before the deposition of the upper or cap layer. Therefore, rapid sedimentation cannot be considered as a catalyst agent (see Figure 8). The impact-induced shaking contributes to the sediment liquefaction process [88]. The absence of impact events has been observed in the study area due to shaking of the impact.

The large scale of the deformation structures reported in Figures 4A and 7A indicated that they were exposed to a large amount of liquefaction. This phenomenon only occurs as a response to a large earthquake that deforms the entire layer. The vertical repetition of the deformed layers overlain by undeformed layers (Figure 4) indicates an irregular shaking corresponding to the periods of earthquakes. The layers including a deformation structure that developed laterally and vertically were the evidence of these soft sediments that occurred due to seismic shocks (Figure 4). Several manifestations of water passages including the passage of sand (Figure 6A) and folds were interpreted as being caused by earthquakes in the same study area [7], named Detachment Folds (Figure 4).

In the comprehensive examination of the deformed sediments within the Lisan Formation on the western side of the DSB, researchers observed a convergence towards the center of the basin, as documented by Alsop et al. [61]. Conversely, other sediments were observed to trend towards the east, specifically towards lower elevations (Figure 1A). On the eastern side of the DSB, after tracing layers across multiple locations, it became apparent that when observed as an outcrop, the general orientation of folds within the distorted layers exhibited a predominantly north–south trend, with some deviations towards the south. This deviation from the central axis of the DSB is attributed to various dips experienced by the region. Furthermore, when examined in an east–west direction, the folds within the deformed layers displayed a tendency towards the west, consistent with findings from the western portion of the DSB.

Several faults affecting the Quaternary sediments within the Lisan Formation, including the Lisan Marl and Lisan Marl gravel, at various locations were measured (Figure 10A–D). These measurements involved strike and dip assessments to understand the relationship between these faults and major fault systems, specifically the DSTF, the Karak Wadi Al Fayha Fault (a transtensional fault system [88]), and the Ed Dhira'a Fault (a transpressional fault system [89]). The results showed that many of these faults displayed NNW–SSE-striking normal and reverse faults, aligning with the overall trend of the DSTF in the study area, which deviates from its typical N–S strike-slip fault [90]. Additionally, measurements at other locations indicated that local faults generally trended NW–SE, consistent with the orientation of the Karak Wadi Al Fayha Fault [86] (Figure 11A,B).

It is worth noting that the faults in Figure 10A,C are N–S-striking transtensional faults, aligning with the direction of the DSTF, while those in Figure 10B,D are N–S-trending normal faults. These faults impacted Quaternary period sediments, indicating that the DSTF remained active.

In a comparable geological context, SSDS investigations have been carried out in the Dexi paleolake near the eastern boundary of the Tibetan Plateau, along the upper reaches of the Mijiang River [85]. The Dexi paleolake lies within one of the most seismically active regions globally, and findings suggest that SSDS occurrences are linked to seismic events with magnitudes of $\geq$5.5 ML in the area [91], similar to the Dead Sea.

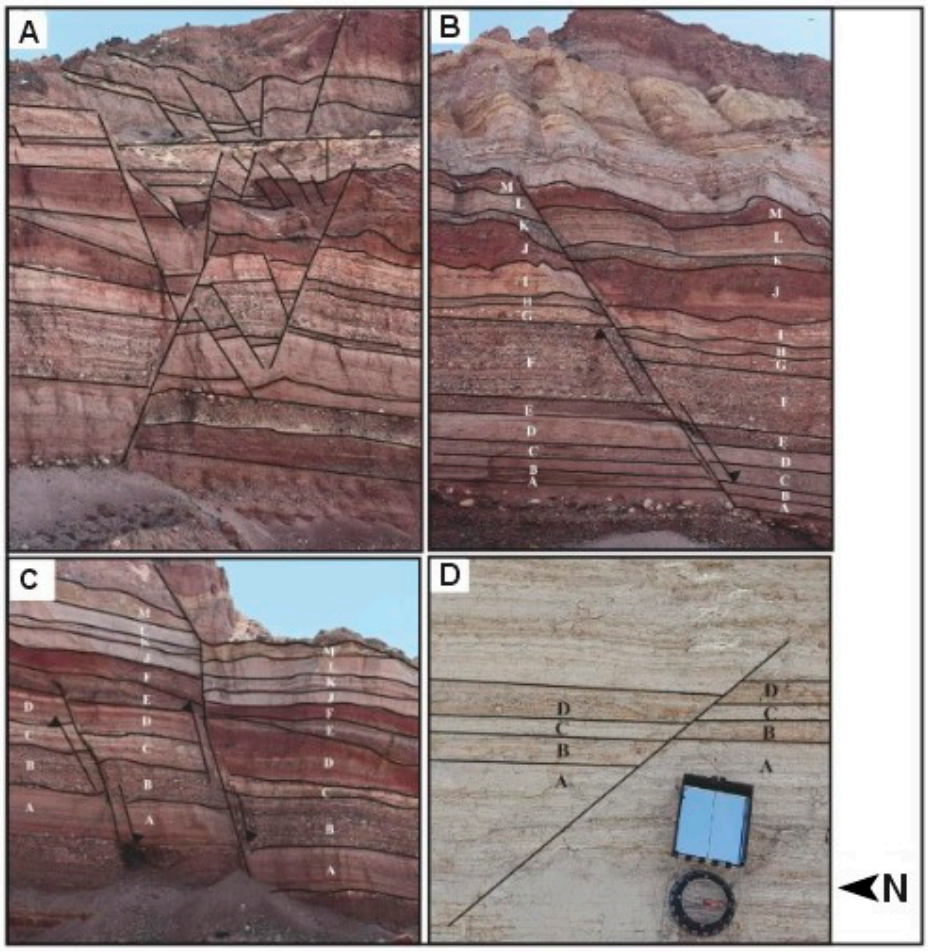

Figure 10. (**A**) A transtensional fault system comprising several normal faults that intersect the Quaternary deposits (the Lisan Formation), forming a negative-flower structure. (**B**–**D**) (31°5′44.20″ N, 35°31′31.00″ E; site 1) and (31°13′35.10″ N, 35°31′28.00″ E; site 8).

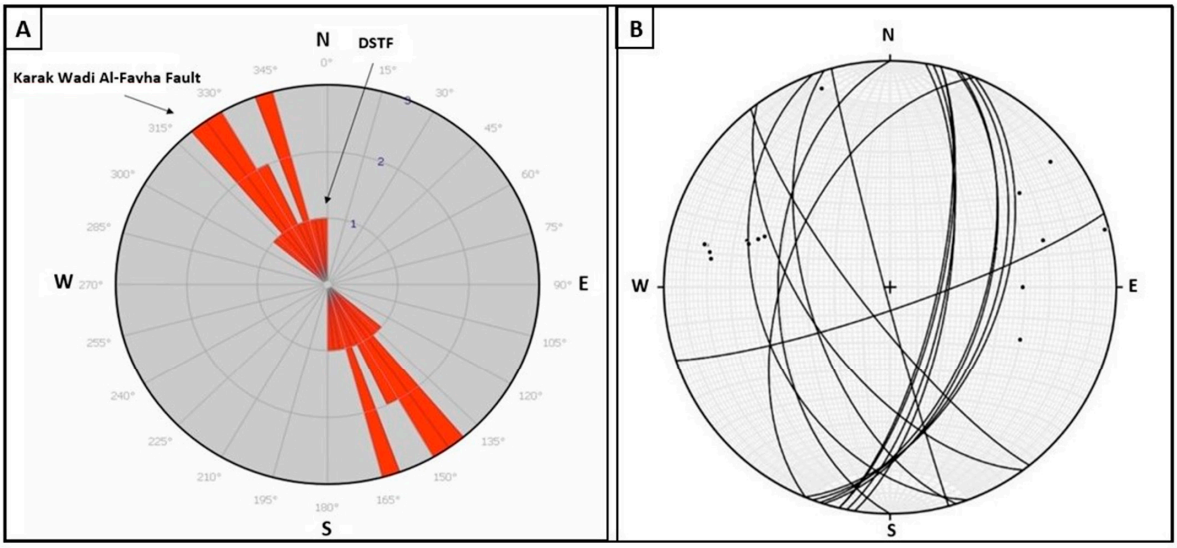

Figure 11. (**A**) Rose diagram showing the faults measurements and indicating the correspondence with the DSTF and the Karak Wadi Al Fayha Fault. (**B**) Cyclographs and poles (dots) of the faults (dots).

6. Conclusions

In the Dead Sea region, SSDSs are abundant and exceptionally well preserved due to unique geological and environmental factors, including rapid sedimentation rates and seismic activity. The region, influenced by the DSTF, offers valuable insights into tectonic activity and historical earthquakes predating modern instrumentation. Seismic activity and rapid sedimentation during the Pleistocene period characterize the sedimentological record of the Dead Sea region, impacting the formation of SSDSs.

This study reports on the sedimentological analysis of SSDSs from the Dead Sea area in Jordan. Nineteen outcrops near the Lisan Peninsula, where the prominent Lisan Formation exposes numerous deformations, were investigated sedimentologically, stratigraphically, and structurally. Mineralogical and geochemical analyses, utilizing XRD and XRF techniques, identified aragonite and halite as predominant minerals, with $CaCO_3$ and NaCl as the dominant elements. The similarity in chemical and mineralogical components in both deformed and undeformed layers indicates that the seisemites along the Dead Sea Basin were formed due to earthquakes.

Field observations, combined with mineralogical and geochemical data, suggest tectonic activity as the primary driver of SSDS formation in the Dead Sea region. We tentatively propose that the SSDSs in the DSB are likely products of earthquakes with magnitudes $\geq$5.5 ML, as the area is seismically active. Additionally, factors such as high salinity, arid climate, and specific depositional settings may have contributed to their formation. These structures provide valuable insights into the geological history, environmental conditions, and tectonic evolution of the region.

Author Contributions: B.S.A.-S., M.A. and M.A.H.: investigation, conceptualization, methodology, validation, and writing—original draft preparation; T.A.Q., D.S. and E.A.: writing—review and editing. All authors have read and agreed to the published version of the manuscript.

Funding: This research received no external funding.

Data Availability Statement: Data are available on request from the corresponding authors.

Acknowledgments: The authors would like to thank Yousef Abu Salha (Department of Geology, the University of Jordan) and Tareq Al Bashiti (Department of Earth Science and Environment, the Hashemite University) for analyzing the XRF and XRD samples and interpreting the results.

Conflicts of Interest: The work described in this manuscript was not published previously, it is not under consideration for publication elsewhere, and its publication is tacitly approved by all the authors. Therefore, the authors declare no conflicts of interest.

References

1. Seilacher, A. Fault-graded beds interpreted as seismites. *Sedimentology* **1969**, *13*, 155–159. [CrossRef]
2. Plaziat, J.; Ahmamou, M. Les Différents Mécanismes à l'Origine de La Diversité Des Séismites, Leur Identification Dans Le Pliocène Du Saïss de Fès et de Meknès (Maroc) et Leur Signification Tectonique. *Geodin. Acta* **1998**, *11*, 183–203. [CrossRef]
3. Montenat, C.; Barrier, P.; Ott d'Estevou, P.; Hibsch, C. Seismites: An Attempt at Critical Analysis and Classification. *Sediment. Geol.* **2007**, *196*, 5–30. [CrossRef]
4. Owen, G.; Moretti, M. Determining the Origin of Soft-Sediment Deformation Structures: A Case Study from Upper Carboniferous Delta Deposits in South-West Wales, UK. *Terra Nova* **2008**, *20*, 237–245. [CrossRef]
5. Owen, G.; Moretti, M.; Alfaro, P. Recognising Triggers for Soft-Sediment Deformation: Current Understanding and Future Directions. *Sediment. Geol.* **2011**, *235*, 133–140. [CrossRef]
6. Ezquerro, L.; Moretti, M.; Liesa, C.L.; Luzón, A.; Múñoz, L. Seismites from a Well Core of Palustrine Deposits as a Tool for Reconstructing the Palaeoseismic History of a Fault. *Tectonophysics* **2015**, *655*, 191–205. [CrossRef]
7. El-Isa, Z.H.; Mustafa, H. Earthquake Deformations in the Lisan Deposits and Seismotectonic Implications. *Geophys. J. Int.* **1986**, *86*, 413–424. [CrossRef]
8. Rossetti, D.D.F. Soft-Sediment Deformation Structures in Late Albian to Cenomanian Deposits, Sao Luis Basin, Northern Brazil: Evidence for Palaeoseismicity. *Sedimentology* **1999**, *46*, 1065–1081. [CrossRef]
9. Van Loon, A.J. Soft-Sediment Deformation Structures in Siliciclastic Sediments: An Overview. *Geologos* **2009**, *15*, 3–55.

10. Moretti, M.; Alfaro, P.; Owen, G. The Environmental Significance of Soft-Sediment Deformation Structures: Key Signatures for Sedimentary and Tectonic Processes. *Sediment. Geol.* **2016**, *344*, 1–4. [CrossRef]
11. Amaireh, M. Overpressure and Liquefaction in the Recent Deposition of the Dead Sea and Resulting Features. Master's Thesis, The University of Jordan, Amman, Jordan, 2017. *Unpublished*.
12. Allen, J.R.L. The Plan Shape of Current Ripples in Relation to Flow Conditions. *Sedimentology* **1977**, *24*, 53–62. [CrossRef]
13. Allen, J.R.L. *Sedimentary Structures: Their Character and Physical Basis*; Elsevier Scientific Pub. Co.: New York, NY, USA, 1982; ISBN 9780444419354.
14. Owen, G. Deformation Processes in Unconsolidated Sands. *Geol. Soc. Lond. Spec. Publ.* **1987**, *29*, 11–24. [CrossRef]
15. Agnon, A.; Migowski, C.; Marco, S. Intraclast Breccia Layers in Laminated Sequences: Recorders of Paleo-Earthquakes. *Geol. Soc. Am. Spec. Publ.* **2006**, *401*, 195–214. [CrossRef]
16. Greb, S.F.; Archer, A.W. Soft-Sediment Deformation Produced by Tides in a Meizoseismic Area, Turnagain Arm, Alaska. *Geology* **2007**, *35*, 435. [CrossRef]
17. Moretti, M.; van Loon, A.T.; Liu, M.; Wang, Y. Restrictions to the Application of "Diagnostic" Criteria for Recognizing Ancient Seismites. *J. Palaeogeogr.* **2014**, *3*, 162–173. [CrossRef]
18. Feng, Z.Z.; Bao, Z.D.; Zheng, X.J.; Wang, Y. Researches of Soft-Sediment Deformation Structures and Seismites in China—A brief Review. *J. Palaeogeogr.* **2016**, *5*, 311–317. [CrossRef]
19. Hibsch, C.; Alvarado, A.; Yepes, H.; Perez, V.H.; Sébrier, M. Holocene liquefaction and soft-sediment deformation in Quito (Ecuador): A paleoseismic history recorded in lacustrine sediments. *J. Geodyn.* **1997**, *24*, 259–280. [CrossRef]
20. Mohindra, R.; Bagati, T.N. Seismically induced soft-sediment deformation structures (seismites) around Sumdo in the lower Spiti valley (Tethys Himalaya). *Sediment. Geol.* **1996**, *101*, 69–83. [CrossRef]
21. Seilacher, A. Sedimentary Structures Tentatively Attributed to Seismic Events. *Mar. Geol.* **1984**, *55*, 1–12. [CrossRef]
22. Lowe, D.R. Water Escape Structures in Coarse-Grained Sediments. *Sedimentology* **1975**, *22*, 157–204. [CrossRef]
23. Seth, A.; Sarkar, S.; Bose, P.K. Synsedimentary Seismic Activity in an Immature Passive Margin Basin (Lower Member of the Katrol Formation, Upper Jurassic, Kutch, India). *Sediment. Geol.* **1990**, *68*, 279–291. [CrossRef]
24. Pratt, B.R. Seismites in the Mesoproterozoic Altyn Formation (Belt Supergroup), Montana: A Test for Tectonic Control of Peritidal Carbonate Cyclicity. *Geology* **1994**, *22*, 1091. [CrossRef]
25. Van Loon, A.J.; Pisarska-Jamroży, M. Sedimentological Evidence of Pleistocene Earthquakes in NW Poland Induced by Glacio-Isostatic Rebound. *Sediment. Geol.* **2014**, *300*, 1–10. [CrossRef]
26. Enzel, Y.; Amit, R.; Dayan, U.; Crouvi, O.; Kahana, R.; Ziv, B.; Sharon, D. The Climatic and Physiographic Controls of the Eastern Mediterranean over the Late Pleistocene Climates in the Southern Levant and Its Neighboring Deserts. *Glob. Planet. Change* **2008**, *60*, 165–192. [CrossRef]
27. Torfstein, A.; Enzel, Y. Dead Sea lake level changes and Levant palaeoclimate. In *Quaternary of the Levant: Environments, Climate Change, and Humans*; Cambridge University Press: Cambridge, UK, 2017; pp. 115–126.
28. Garfunkel, Z. Internal Structure of the Dead Sea Leaky Transform (Rift) in Relation to Plate Kinematics. *Tectonophysics* **1981**, *80*, 81–108. [CrossRef]
29. Donahue, J. The Dead Sea: The Lake and Its Setting. By Tina M. Niemi, Zvi Ben-Avraham, and Joel R. Gat. *Am. J. Archaeol.* **1999**, *103*, 3. [CrossRef]
30. Ben Dor, Y.; Neugebauer, I.; Enzel, Y.; Schwab, M.H.; Tjallingii, R.; Erel, Y.; Brauer, A. Varves of the Dead Sea Sedimentary Record. *Quat. Sci. Rev.* **2019**, *1*, 173–184. [CrossRef]
31. Atallah, M. Tectonic evolution of northern Wadi Araba, Jordan. *Tectonophysics* **1992**, *204*, 17–26. [CrossRef]
32. Al Hseinat, M.; Al-Rawabdeh, A.; Al-Zidaneen, M.; Ghanem, H.; Al-Taj, M.; Diabat, A.; Jarrar, G.; Atallah, M. New Insights for Understanding the Structural Deformation Style of the Strike-Slip Regime along with the Wadi Shueib and Amman-Hallabat Structures in Jordan Based on Remote Sensing Data Analysis. *Geosciences* **2020**, *10*, 253. [CrossRef]
33. Stern, R.J.; Johnson, P. Continental Lithosphere of the Arabian Plate; a Geologic, Petrologic, and Geophysical Synthesis. *Earth-Sci. Rev.* **2010**, *101*, 29–67. [CrossRef]
34. Quennell, A.M. *The Geology and Mineral Resources of (Former) Trans-Jordan*; HM Stationery Office: England, UK, 1951.
35. Garfunkel, Z.; Zak, Y.; Freund, R. Active faulting in the Dead Sea rift. *Tectonophysics* **1981**, *80*, 1–26. [CrossRef]
36. Hempton, M. Constraints on Arabian plate motion and extensional history of the Red Sea. *Tectonics* **1987**, *6*, 687–705. [CrossRef]
37. Lu, Y.; Bookman, R.; Waldmann, N.; Marco, S. A 45 kyr laminae record from the Dead Sea: Implications for basin erosion and floods recurrence. *Quat. Sci. Rev.* **2020**, *229*, 106143. [CrossRef]
38. Quennell, A.M. The structural and geomorphic evolution of the Dead Sea Rift. *Q. J. Geol. Soc.* **1958**, *114*, 1–24. [CrossRef]
39. Freund, R.; Garfunkel, Z.; Zak, I.; Goldberg, M.; Weissbrod, T.; Derin, B.; Girdler, R.W. The shear along the Dead Sea rift. *Philos. Trans. R. Soc. London. Ser. A Math. Phys. Sci.* **1970**, *267*, 107–130.
40. Letouzey, J.; Tremolieres, P. Paleo-stress fields around the Mediterranean since the Mesozoic from microtectonics. Comparison with plate tectonic data. In *Tectonic Stresses in the Alpine-Mediterranean Region: Proceedings of the Symposium Held in Vienna, Austria, 13–14 September 1979*; Springer: Vienna, Austria, 1980; pp. 173–192.
41. Segev, A.; Lyakhovsky, V.; Weinberger, R. Continental Transform–Rift Interaction Adjacent to a Continental Margin: The LevantCase Study. *Earth-Sci. Rev.* **2014**, *139*, 83–103. [CrossRef]

42. Schattner, U.; Ben-Avraham, Z.; Reshef, M.; Bar-Am, G.; Lazar, M. Oligocene–Miocene Formation of the Haifa Basin: Qishon–Sirhan Rifting Coeval with the Red Sea–Suez Rift System. *Tectonophysics* **2006**, *419*, 1–12. [CrossRef]
43. Hofmann, C.; Courtillot, V.; Féraud, G.; Rochette, P.; Yirgu, G.; Ketefo, E.; Pik, R. Timing of the Ethiopian Flood Basalt Event and Implications for Plume Birth and Global Change. *Nature* **1997**, *389*, 838–841. [CrossRef]
44. Shimon Ilani, S.; Yehudit Harlavan, Y.; Khalid Tarawneh, K.; Rabba, I.; Weinberger, R.; Ibrahim, K.; Peltz, S.; Steinitz, G. New K-591 Ar Ages of Basalts from the Harrat Ash Shaam Volcanic Field in Jordan: Implications for the Span and Duration of the Upper-Mantle Upwelling beneath the Western Arabian Plate. *Geology* **2001**, *29*, 171. [CrossRef]
45. Pik, R.; Marty, B.; Carignan, J.; Lavé, J. Stability of the Upper Nile Drainage Network (Ethiopia) Deduced from (U–Th)/He Thermochronometry: Implications for Uplift and Erosion of the Afar Plume Dome. *Earth Planet. Sci. Lett.* **2003**, *215*, 73–88. [CrossRef]
46. Segev, A.; Rybakov, M. History of Faulting and Magmatism in the Galilee (Israel) and across the Levant Continental Margin Inferred from Potential Field Data. *J. Geodyn.* **2011**, *51*, 264–284. [CrossRef]
47. Avni, Y.; Segev, A.; Ginat, H. Oligocene Regional Denudation of the Northern Afar Dome: Pre- and Syn-Breakup Stages of the Afro-Arabian Plate. *Geol. Soc. Am. Bull.* **2012**, *124*, 1871–1897. [CrossRef]
48. Faccenna, C.; Becker, T.W.; Jolivet, L.; Keskin, M. Mantle Convection in the Middle East: Reconciling Afar Upwelling, Arabia Indentation and Aegean Trench Rollback. *Earth Planet. Sci. Lett.* **2013**, *375*, 254–269. [CrossRef]
49. Wald, R.; Schattner, U. Initiation of Arabian Plate Exposure during the Oligocene, Evidence from the Galilee, Israel. In Proceedings of the International Conference & Exhibition, Istanbul, Turkey, 17 September 2014.
50. Bartov, Y.; Stein, M.; Enzel, Y.; Agnon, A.; Reches, Z. Lake Levels and Sequence Stratigraphy of Lake Lisan, the Late Pleistocene Precursor of the Dead Sea. *Quat. Res.* **2002**, *57*, 9–21. [CrossRef]
51. Al-Saqarat, B.S.; Abbas, M.; Lai, Z.; Gong, S.; Alkuisi, M.M.; Abu Hamad, A.M.B.; Carling, P.A.; Jansen, J.D. A Wetland Oasis at Wadi Gharandal Spanning 125–70 Ka on the Human Migration Trail in Southern Jordan. *Quat. Res.* **2020**, *100*, 154–169. [CrossRef]
52. Abbas, M.; Lai, Z.; Jansen, J.D.; Tu, H.; Alqudah, M.; Xu, X.; Al-Saqarat, B.S.; Mu'ayyad Al Hseinat; Ou, X.; Petraglia, M.D.; et al. Human Dispersals out of Africa via the Levant. *Sci. Adv.* **2023**, *9*, eadi6838. [CrossRef]
53. Waldmann, N.; Stein, M.; Ariztegui, D.; Starinsky, A. Stratigraphy, Depositional Environments and Level Reconstruction of the Last Interglacial Lake Samra in the DSB. *Quat. Res.* **2009**, *72*, 1–15. [CrossRef]
54. Torfstein, A.; Goldstein, S.L.; Kagan, E.J.; Stein, M. Integrated Multi-Site U–Th Chronology of the Last Glacial Lake Lisan. *Geochim. Et Cosmochim. Acta* **2013**, *104*, 210–231. [CrossRef]
55. Landmann, G.; Abu Qudaira, G.M.; Shawabkeh, K.; Wrede, V.; Kempe, S. Geochemistry of the Lisan and Damya Formations in Jordan, and Implications for Palaeoclimate. *Quat. Int.* **2002**, *89*, 45–57. [CrossRef]
56. Haase-Schramm, A.; Goldstein, S.L.; Stein, M. U-Th Dating of Lake Lisan (Late Pleistocene Dead Sea) Aragonite and Implications for Glacial East Mediterranean Climate Change. *Geochim. Cosmochim. Acta* **2004**, *68*, 985–1005. [CrossRef]
57. Abed, A.M.; Yaghan, R. On the paleoclimate of Jordan during the last glacial maximum. *Palaeogeogr. Palaeoclimatol. Palaeoecol.* **2000**, *160*, 23–33. [CrossRef]
58. Migowski, C.; Stein, M.; Prasad, S.; Negendank, J.F.W.; Agnon, A. Holocene Climate Variability and Cultural Evolution in the 550 near East from the Dead Sea Sedimentary Record. *Quat. Res.* **2006**, *66*, 421–431. [CrossRef]
59. Kiro, Y.; Goldstein, S.L.; Lazar, B.; and Stein, M. Environmental implications of salt facies in the Dead Sea. *Bulletin* **2016**, *128*, 5–6, 824–841. [CrossRef]
60. Alsop, G.I.; Weinberger, R.; Marco, S.; Levi, T. Folding during soft-sediment deformation. *Geol. Soc. Lond. Spec. Publ.* **2020**, *487*, 81–104. [CrossRef]
61. Heifetz, E.; Agnon, A.; Marco, S. Soft Sediment Deformation by Kelvin Helmholtz Instability: A Case from Dead Sea Earthquakes. *Earth Planet. Sci. Lett.* **2005**, *236*, 497–504. [CrossRef]
62. Drazin, P.G.; Reid, W.H. *Darlene Reid Hydrodynamic Stability*; Cambridge University Press: Cambridge, UK, 2004. [CrossRef]
63. Marco, S.; Stein, M.; Agnon, A.; Ron, H. Long-Term Earthquake Clustering: A 50,000-Year Paleoseismic Record in the Dead Sea Graben. *J. Geophys. Res. Solid Earth* **1996**, *101*, 6179–6191. [CrossRef]
64. Lowe, D.R.; LoPiccolo, R.D. The Characteristics and Origins of Dish and Pillar Structures. *J. Sediment. Res.* **1974**, *44*, 484–501. [CrossRef]
65. LOWE, D.R. Subaqueous Liquefied and Fluidized Sediment Flows and Their Deposits. *Sedimentology* **1976**, *23*, 285–308. [CrossRef]
66. Cosgrove, J.W. The Expression of Hydraulic Fracturing in Rocks and Sediments. *Geol. Soc. Lond. Spec. Publ.* **1995**, *92*, 187–196. [CrossRef]
67. Levi, T.; Weinberger, R.; Aïfa, T.; Eyal, Y.; Marco, S. Injection Mechanism of Clay-Rich Sediments into Dikes during Earthquakes. *Geochem. Geophys. Geosystems* **2006**, *7*, 12. [CrossRef]
68. Levi, T.; Weinberger, R.; Eyal, Y.; Lyakhovsky, V.; Heifetz, E. Velocities and Driving Pressures of Clay-Rich Sediments Injected into Clastic Dykes during Earthquakes. *Geophys. J. Int.* **2008**, *175*, 1095–1107. [CrossRef]
69. Moretti, M.; Sabato, L. Recognition of Trigger Mechanisms for Soft-Sediment Deformation in the Pleistocene Lacustrine Deposits of the Sant'Arcangelo Basin (Southern Italy): Seismic Shock vs. Overloading. *Sediment. Geol.* **2007**, *196*, 31–45. [CrossRef]
70. Owen, G. Load Structures: Gravity-Driven Sediment Mobilization in the Shallow Subsurface. *Geol. Soc. Lond. Spec. Publ.* **2003**, *216*, 21–34. [CrossRef]

71. Wang, P.; Zhang, B.; Qiu, W.-L.; Jian-cun, W. Soft-Sediment Deformation Structures from the Diexi Paleo-Dammed Lakes in the Upper Reaches of the Minjiang River, East Tibet. *J. Asian Earth Sci.* **2011**, *40*, 865–872. [CrossRef]
72. Alsop, G.I.; Marco, S. Tsunami and Seiche-Triggered Deformation within Offshore Sediments. *Sediment. Geol.* **2012**, *261–262*, 90–107. [CrossRef]
73. Prasad, S.; Vos, H.; Negendank, J.F.W.; Waldmann, N.; Goldstein, S.L.; Stein, M. Evidence from Lake Lisan of Solar Influence on Decadal- to Centennial-Scale Climate Variability during Marine Oxygen Isotope Stage 2. *Geology* **2004**, *32*, 581–584. [CrossRef]
74. Prasad, S.; Negendank, J.F.W.; Stein, M. Varve Counting Reveals High Resolution Radiocarbon Reservoir Age Variations in Palaeolake Lisan. *J. Quat. Sci. Publ. Quat. Res. Assoc.* **2009**, *24*, 690–696. [CrossRef]
75. Migowski, C.; Agnon, A.; Bookman, R.; Negendank, J.F.; Stein, M. Recurrence Pattern of Holocene Earthquakes along the Dead Sea Transform Revealed by Varve-Counting and Radiocarbon Dating of Lacustrine Sediments. *Earth Planet. Sci. Lett.* **2004**, *222*, 301–314. [CrossRef]
76. Sims, J.D. Determining Earthquake Recurrence Intervals from Deformational Structures in Young Lacustrine Sediments. *Tectonophysics* **1975**, *29*, 141–152. [CrossRef]
77. Scott, B.C.; Price, S.J. Earthquake-Induced Structures in Young Sediments. *Tectonophysics* **1988**, *147*, 165–170. [CrossRef]
78. Maltman, A.J.; Bolton, A. How Sediments Become Mobilized. *Geol. Soc. Lond. Spec. Publ.* **2003**, *216*, 9–20. [CrossRef]
79. Alvarez, W.; Staley, E.; O'Connor, D.; Chan, M.A. Synsedimentary Deformation in the Jurassic of Southeastern Utah—A Case of Impact Shaking? *Geology* **1998**, *26*, 579–582. [CrossRef]
80. Alfaro, P.; Delgado, J.; Estévez, A.; Molina, J.M.; Moretti, M.; Soria, J.M. Liquefaction and Fluidization Structures in Messinian Storm Deposits (Bajo Segura Basin, Betic Cordillera, Southern Spain). *Int. J. Earth Sci.* **2002**, *91*, 505–513. [CrossRef]
81. Weaver, L.; Arnaud, E. Polyphase Glacigenic Deformation in the Waterloo Moraine, Kitchener, Ontario, Canada. *Sediment. Geol.* **2011**, *235*, 292–303. [CrossRef]
82. Arnaud, E. The Paleoclimatic Significance of Deformation Structures in Neoproterozoic Successions. *Sediment. Geol.* **2012**, *243–244*, 33–56. [CrossRef]
83. Ravier, E.; Buoncristiani, J.-F.; Guiraud, M.; Menzies, J.; Clerc, S.; Goupy, B.; Portier, E. Porewater Pressure Control on Subglacial Soft Sediment Remobilization and Tunnel Valley Formation: A Case Study from the Alnif Tunnel Valley (Morocco). *Sediment. Geol.* **2014**, *304*, 71–95. [CrossRef]
84. Wetzler, N.; Marco, S.; Heifetz, E. Quantitative analysis of seismogenic shear-induced turbulence in lake sediments. *Geology* **2010**, *38*, 303–306. [CrossRef]
85. Li, J.; Jansen, J.; Carling, P.; Çiner, A.; Fan, X. Soft-sediment deformation structures within a 166 m-long drill core from Diexi Palaeolake, eastern Tibetan Plateau. *Sediment. Geol.* 2024; *to be Submitted*.
86. Alsop, G.I.; Weinberger, R.; Marco, S.; Levi, T. Identifying Soft-Sediment Deformation in Rocks. *J. Struct. Geol.* **2019**, *125*, 248–255. [CrossRef]
87. Qutishat, T. Active Tectonic Movement of the Dead Sea Transform Fault Induced Soft-Sediments Deformation: Instances from the Quaternary Deposits at Wadi Al-Alkharazeh. Master's Thesis, The University of Jordan, Amman, Jordan, 2022; pp. 1–180.
88. Al Hseinat, M.; AlZidaneen, M.; Jaradat, R.; Al-Rawabdeh, A.; Hübscher, C. Tectono-Stratigraphic Framework and Evolution of the Northwestern Arabian Plate, Central Jordan. *Tectonophysics* **2023**, *863*, 229993. [CrossRef]
89. Abed, A.M. *The Geology of Jordan and Its Environment and Water*; Scientific Series 1; Publication of Association of Jordanian Geologists: Amman, Jordan, 2000; 571p. (In Arabic)
90. Powell, J.H. *The Geology of the Karak Area, Map Sheet No. 3152 III*; Geology Directorate, Natural Resources Authority: Amman, Jordan, 1988; p. 171.
91. Mart, Y.; Vachtman, D. The Internal Grabens of the Levant Rifts and Their Geodynamic Significance. *Comptes Rendus Geoscience* **2015**, *347*, 191–200. [CrossRef]